

Clogging in parallelized tapered microfluidic channels

Sorell S. Massenburg¹ · Esther Amstad² · David A. Weitz¹

Received: 23 February 2016 / Accepted: 23 May 2016 / Published online: 11 June 2016
© Springer-Verlag Berlin Heidelberg 2016

Abstract Nearly all tubes and pores used to transport solids in fluids, such as arteries and filters, are subject to clogging. The length scales and geometries of these tubes are well defined. In spite of this knowledge, the collective clogging behavior of multiple tubes has not yet been connected to their shapes and sizes. We investigate the clogging behavior of ten parallel tubes, which we model with ten parallel tapered microchannels using poly(styrene) beads to induce clogging events. The clogging behavior depends on the channel geometry as well as the shear stress particles are subjected to. Although our microchannels model filters, our results can be applied to the clogging behavior of a broad range of applications such as the clogging in arteries, inkjets, or xylem in trees.

Keywords Microfluidics · Clogging · Particle suspension

1 Introduction

The obstruction of flow due to clogging can cause failure in any industrial or technological process that involves the transport of solids suspended in a liquid. For example, clogging can negatively affect oil recovery, 3-D printing processes, or even blood circulation in the body. However, clogging can also be useful: In many filtration processes, the clogging of porous membranes removes particulates

from solutions and thus desired. Therefore, a physical understanding of clogging is essential for both its prevention and its utilization.

Clogging can occur when a particle flows into a pore that is smaller than the particle size. Clogging can also occur when particles smaller than the pore aggregate in solution. In addition, clogging can be induced by an accumulation of particles on the pore surface. In this case, the degree of accumulation depends on the ratio of the force attracting the particles to the channel walls to the shear forces that hinder particles from adsorption on the channel wall (Henry et al. 2012). This interplay between attractive and repulsive forces can be studied by flowing model particle suspensions through microchannels. This has been done in great detail for uniformly varying microfluidic channels: In this case, clogging depends on the channel size, particle size, and the number of particles that flow past the smallest constriction (Wyss et al. 2006; Mustin and Stoeber 2010; Henry et al. 2012; Sauret et al. 2014; Bacchin et al. 2013). However, in many cases, the pore width decreases over the length of the pore; for example, the width of arteries can vary by more than an order of magnitude (Kumar et al. 2014). Moreover, the pore size in filter membranes often varies over the length of the membrane. Pores with varying widths clog through a different mechanism (Tobiason and Vigneswaran 1994). However, the clogging behavior of parallelized converging microchannels has never been studied.

In this paper, we investigate clogging in parallelized converging microchannels using a dispersion of electrostatically stabilized colloids. The propensity of channels to clog decreases with decreasing hydrodynamic resistance of a channel as this increases the flow rate of the fluid and hence the shear stress that particles experience.

✉ Sorell S. Massenburg
massenb2@fas.harvard.edu

¹ Harvard University School of Engineering and Applied Sciences, Cambridge, MA, USA

² Institute of Materials, École Polytechnique Fédérale de Lausanne (EPFL), Lausanne, Switzerland

2 Materials and methods

Using compressed air, we push a particulate suspension through tubing past two pressure transducers (Omega PX409), into a microfluidic device and out to a waste container held at atmospheric pressure, as schematically shown in Fig. 1a. To more closely mimic filters, we study the clogging behavior of parallelized microchannels. We limit the number of channels in the array to ten to enable simultaneous observation of each individual microchannel with optical microscopy. We fabricate microchannel arrays with variable width from poly(dimethylsiloxane) (PDMS) using standard soft lithography (Duffy et al. 1998). Each channel has a mouth of width, (W_m), where fluid enters the channel and the mouth tapers to a constriction width, that we keep constant at 10 μm , as shown in Fig. 1b. We vary the mouth width between 100 and 20 μm and the channel length, L , between 1200 and 300 μm . To ensure that the wettability of all the channel walls is the same and remains stable over time, we bond PDMS channels to a PDMS surface using the soft bake method (Eddings et al. 2008) and avoid the oxygen plasma bonding that is much more commonly used (Shun'ko and Belkin 2012).

Polystyrene microbeads (Thermo Fischer Scientific—C37281) are dispersed in a mixture of 63 % water and 37 vol% heavy water(VWR), and we use this mixture of solvents to match the density of the suspending solution to the dispersed microbeads. Monodisperse microbeads with 3 μm diameters are dispersed at 4 % (v/v) (2.8×10^9 particles/mL). To avoid spontaneous aggregation in solution,

the microbeads are electrostatically stabilized with carboxyl groups. The microbead dispersion is flowed through the microchannel array at a constant pressure. Because the microchannels are arrayed in parallel, the pressure drop experienced across each channel is independent of the other channels.

We initially calculate the flow rate through the microchannel arrays by measuring the pressure difference along a 50-cm-long piece of tubing with a known hydrodynamic resistance (R_H) as shown in Fig. 1a, b. We find the tubing resistance by measuring the pressure difference (ΔP) along the tubing when pure water is flown through the tubing at various flow rates (Q) with a syringe pump according to: $\Delta P = QR_H$ (Oh et al. 2011). The hydrodynamic resistance is the slope of the line fitting the ΔP versus Q graph. The hydrodynamic resistance of the unclogged microchannel array is measured in the same way. The tubing resistance is much lower than the resistance of an unclogged array of microchannels and therefore has little effect on the flow through the microchannel array. Over the course of the experiment, we measure the flow rate through the channel array. Pairing the flow rate measurements with the time each channel requires to clog, we estimate the total volume of particulate suspension that passes through each channel prior to clogging. To estimate the time that each channel takes to clog, we use optical microscopy and time-lapse images (Sony) to monitor the state of each channel in the array during the clogging experiment as shown in Fig. 1c, d.

In addition, we calculate the flow rate through the channels using the pressure applied to the suspension and the

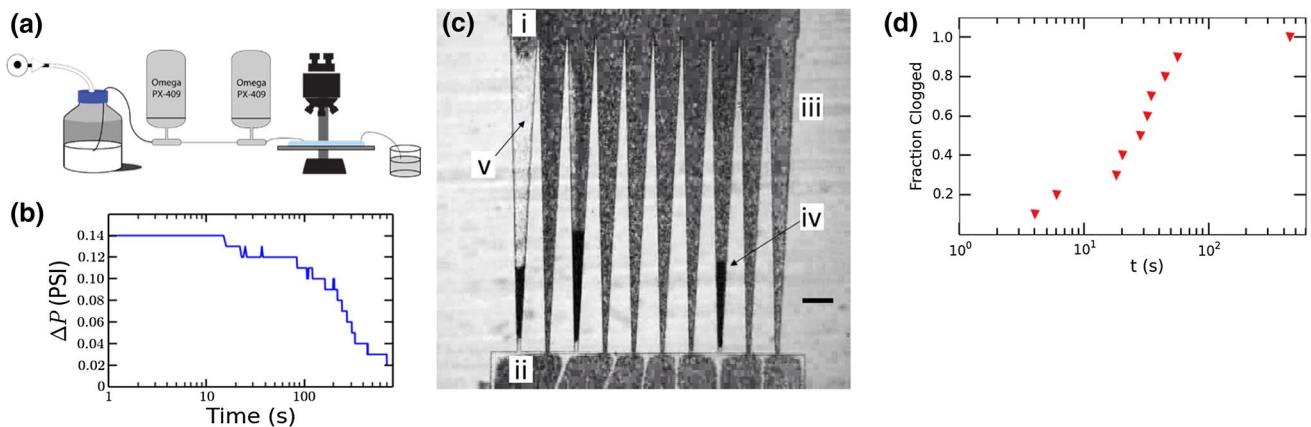


Fig. 1 **a** Schematic of experimental setup used to perform clogging experiments. **b** To quantify fluid flow rates, we measure the pressure drop across the tubing during the clogging experiments. We convert the pressure drop into a flow rate using the hydrodynamic resistance of the tubing that we experimentally determine with control experiments. Measured pressure difference across resistance tubing during a the clogging of an array of 100- to 10- μm channels. **c** Micrograph taken during the clogging of an array of 100- to 10- μm channels. Par-

ticle suspension flows from the *i* mouth width of $W_m = 100 \mu\text{m}$, W_m , to the *ii* exit of width 10 μm . *iii* Gray areas are flowing particulate suspension, *iv* black areas are particle agglomerates that result from clogs, and *v* clear areas inside of the channels contain liquid without particles. Scale bar is 100 μm . **d** Fraction of channels clogged as a function of time during which the particle suspension is flown through an array containing ten channels that taper from 100- to 10- μm channels. **b–d** The same clogging experiment

known channel resistance. Similar to the tubing, we determine the channel resistance by using a syringe pump to flow pure water through the channel array and then measuring the resulting pressure difference across the array. To approximate the resistance of a single channel, we multiply the resistance of the channel array by the number of channels in the array because the channels are parallelized. We track the flow rate through each channel, and we use each channel’s clogging time to estimate the total volume of particulate suspension that passes through each channel prior to clogging.

We calculate the average the flow rate using the two estimates. Although the two estimates are derived from pressure measurements and videos with low temporal resolution (1 measurement per second), they nonetheless agree within 50 %. Importantly, both estimates show the same change in clogging behavior in changing taper rate. Using the average flow rate through each channel and the number density of the particulate suspension, we estimate the number of particles that pass through each channel before the channel clogs.

3 Results and discussion

We flow the particle suspension through channels that have 100 μm mouth widths and taper to 10 μm constriction width over a length of 1200 μm, as shown in the optical micrograph in Fig. 1b. The particles adsorb at the channel walls near the 10 μm constriction leading to a buildup of particles that eventually clog the channel. To investigate the clogging behavior, we measure the fraction of clogged channels over time. It takes 3 s until the first channel clogs, 6 s until the second channel clogs, and as long as 20 s until the third channel clogs. However, once the third channel is clogged, the remaining channels clog very rapidly, as shown by the rapid increase in the percentage of clogged channels with time by the red triangles in Fig. 1d. Using the average of the two flow rate estimates, we approximate the number of particles that pass through the channel prior to clogging.

In non-tapered channels, the number of particles that pass through a constriction before it clogs is proportional to the area of the constriction’s cross section (Wyss et al. 2006). To test whether tapered channels display a similar behavior, we also fabricate channels with a constriction width of 10 μm and mouth widths of 80, 60, 40, and 20 μm. Remarkably, although all the channels have the same constriction width and hence the same cross-sectional area at the constriction, the number of particles that pass

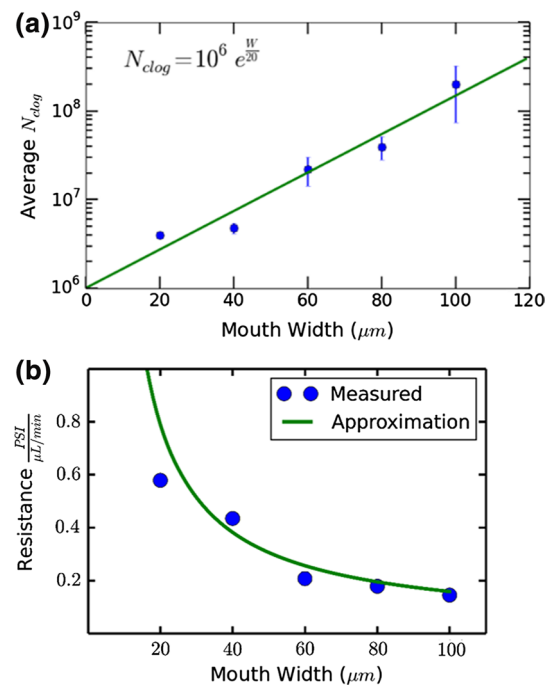


Fig. 2 a N^* versus mouth width plot. b Plot showing hydrodynamic resistance versus mouth width

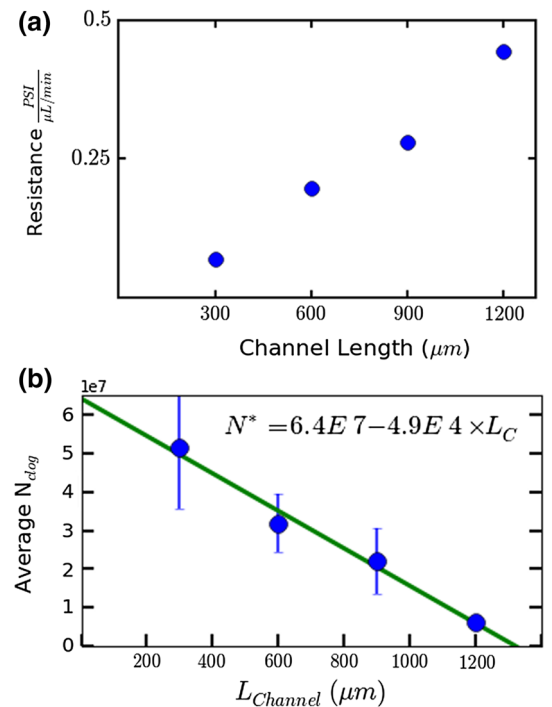


Fig. 3 a Plot showing hydrodynamic resistance versus channel length. b N^* versus channel length for channels with identical taper angle

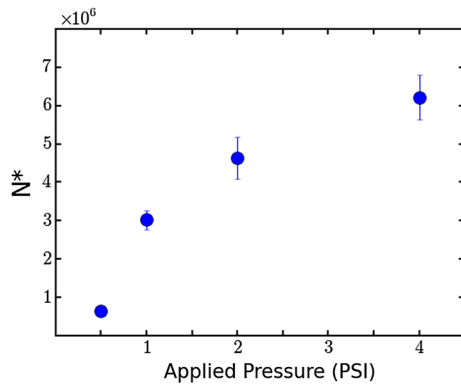


Fig. 4 N^* versus pressure for channels that converge from 40 to 10 μm

through each channel prior to clogging (N^*) exponentially increases with increasing mouth width, as shown in Fig. 2a. To understand the difference in clogging behavior, we quantify the hydrodynamic resistance of each channel type by calculating the slope of the graph of the measured pressure drop (ΔP) across the microfluidic device versus the flow rate (Q) through the device. The hydrodynamic resistance of the channels decreases with increasing mouth width, as shown by the blue circles in Fig. 2b. These experimental results can be fitted with an inverse power law.

Our experiments in channels with variable mouth width simultaneously vary the hydrodynamic resistance and the tapering angle. To separate the influence of these two variables on the clogging behavior, we fabricate channels with decreasing length, and hence with decreasing hydrodynamic resistance, and constant tapering rate. We choose a taper rate that decreases the channel width by 1 μm per 30 μm channel length, which is the same taper rate as the channels whose width decreases from 40 to 10 μm over a length of 1200 μm . Maintaining a constant rate of taper and a constant height of 25 μm , we fabricate three sets of channels: channels that are 900 μm long and have a 33- μm -wide entrance, channels that are 600 μm long and have a 25- μm -wide entrance, and channels that are 300 μm long and have a 18- μm -wide entrance. The hydrodynamic resistance of the channel linearly increases with increasing channel length, as shown in Fig. 4a. Interestingly, the average number of particles that pass through each channel prior to clogging decreases linearly with increasing channel length as shown in Fig. 3b. These results demonstrate that the clogging time is inversely proportional to the hydrodynamic resistance of the channel. As the hydrodynamic resistance of the channel decreases, the fluid velocity in the channel increases, resulting in higher shear stresses that act on particles attached to the walls. Moreover, the higher shear stresses deter particles from approaching and adhering to channel walls. Hence, the probability for particles to

stick to the walls decreases and more particles pass through the constriction before the channel clogs.

Our results suggest that clogging is stymied by increasing the shear stress in the channels. To verify this suggestion, we investigate the influence of shear stress on clogging. We vary the dispersion's flow rate by adjusting the pressure applied to the particulate dispersion. The number of particles that pass through the constriction before clogging increases as the applied pressure increases, as shown in Fig. 4. This result confirms our findings and demonstrates the importance of the shear stress on the propensity of tapered channels to clog. The higher shear stresses inhibit the attachment of particles to the channel walls, thereby delaying channel clogging caused by particle buildup at the channel walls.

4 Conclusions

By flowing particulate dispersions through tapered channels of varying mouth width, channel length and at varying flow rates, we demonstrate that the time needed to clog tapered microchannels depends on the shear stress near the constriction. Increasing a channels mouth width or decreasing its length decreases the hydrodynamic resistance of the channel. As a result, fluid flux through the constriction increases resulting in a higher shear stress near the constriction. These higher shear stresses prevent particles from attaching to the channel walls. This result is consistent with previous findings that reported the clogging behavior to result from a competition between hydrodynamic and surface forces (Henry et al. 2012). A better understanding of the influence of the channel dimension on the clogging behavior is essential to the design of optimized filters and porous networks, which often have variations in pore size. For example, the clogging of nozzles in 3D printers may be delayed by widening the entrance of the nozzle. Moreover, our findings may also help predict clogging in more complicated systems such as blood vessels and porous media.

Acknowledgments The authors would like to thank Onur Kas, Kaare Jensen, Wynter Duncanson and Stephan Koehler for helpful discussions. This work was supported by the National Science Foundation (DMR 1310266) and by the Harvard Materials Research Science and Engineering Center (DMR 1420570).

References

- Bacchin P, Derekx Q, Veyret D, Glucina K, Moulin P (2013) Clogging of microporous channels networks: role of connectivity and tortuosity. *Microfluidics Nanofluidics* 17(1):85–96. doi:10.1007/s10404-013-1288-4
- Duffy DC, McDonald JC, Schueller OJA, Whitesides GM (1998) Rapid prototyping of microfluidic systems in poly(dimethylsiloxane). *Anal Chem* 70(23):4974–4984. doi:10.1021/ac980656z

- Eddings MA, Johnson MA, Gale BK (2008) Determining the optimal PDMS–PDMS bonding technique for microfluidic devices. *J Micromech Microeng* 18(6):067001. <http://stacks.iop.org/0960-1317/18/i=6/a=067001>
- Henry C, Minier J, Lefèvre G (2012) Towards a description of particulate fouling: from single particle deposition to clogging. *Adv Colloid Interface Sci* 185–186. doi:10.1016/j.cis.2012.10.001
- Kumar V, Abbas AK, Fausto N, Aster JC (2014) Robbins and Cotran pathologic basis of disease, 9th edn. Saunders, Philadelphia
- Mustin B, Stoeber B (2010) Deposition of particles from polydisperse suspensions in microfluidic systems. *Microfluidics Nanofluidics* 9(4–5):905–913. doi:10.1007/s10404-010-0613-4
- Oh KW, Lee K, Ahn B, Furlani EP (2011) Design of pressure-driven microfluidic networks using electric circuit analogy. *Lab Chip* 12(3):515–545. doi:10.1039/C2LC20799K
- Sauret A, Barney EC, Perro A, Villermaux E, Stone HA, Dressaire E (2014) Clogging by sieving in microchannels: application to the detection of contaminants in colloidal suspensions. *Appl Phys Lett*. doi:10.1063/1.4893459
- Shun'ko E, Belkin V (2012) Treatment surfaces with atomic oxygen excited in dielectric barrier discharge plasma of O₂ admixed to N₂. *AIP Adv* 2(2):022157
- Tobiason J, Vigneswaran B (1994) Evaluation of a modified model for deep bed filtration. *Water Res* 28(2):335–342
- Wyss HM, Blair DL, Morris JF, Stone HA, Weitz DA (2006) Mechanism for clogging of microchannels. *Phys Rev E* 74(6). doi:10.1103/PhysRevE.74.061402